JOURNAL OF GUIDANCE, CONTROL, AND DYNAMICS
Vol. 18, No. 5, September–October 1995

Aircraft Flight Control in Wind Shear Using Sequential Dynamic Inversion

Sandeep S. Mulgund* and Robert F. Stengel†
Princeton University, Princeton, New Jersey 08544

Longitudinal wind shear flight control laws are developed for the dynamics of a twin-jet transport aircraft using nonlinear dynamic inversion. Time-scale decomposition simplifies controller design by partitioning it into slow and fast time scales. The effects of time-varying winds are explicitly considered in the derivation of the controllers. Three inverting controllers are developed and evaluated: airspeed/climb rate, groundspeed /climb rate, and throttle/climb rate. The implementation of a climb rate scheduling strategy makes it possible for the resultant flight paths to mimic the essential features of optimal escape trajectories developed in an earlier study, where altitude is exchanged for airspeed as a function of microburst strength.

Nomenclature

D = drag, lbf
E_s = specific Energy, ft
F = nondimensional wind shear hazard index
g = acceleration due to gravity, ft/s^2
h = altitude, ft
I_{yy} = moment of inertia about body y axis, slug-ft^2
L = lift, lbf
M = pitching moment
m = mass, slugs
q = pitch rate, rad/s
R = radius of downdraft column, ft
r = rate of climb, ft/s
s = Laplace variable
T = engine thrust, lbf
t = time, s
U_{max} = maximum horizontal wind speed, ft/s
$\boldsymbol{u}$ = aircraft control vector
V_a = airspeed, ft/s
V_i = groundspeed, ft/s
W = weight, lbf
w_x = wind component along the x axis, ft/s
w_h = wind component along the h axis, ft/s
x = distance along the x axis, ft
$\boldsymbol{x}$ = aircraft state vector
$\boldsymbol{y}$ = control system command vector
z_{max} = altitude of maximum outflow, ft
α = angle of attack, rad
γ = flight-path angle, rad
Δ_x = range from core, ft
δ_E = elevator deflection, deg
δ_T = throttle setting, %
θ = pitch attitude, rad

Subscripts

a, A = air-mass referenced quantity
c = commanded value
i, I = inertially referenced quantity

Superscript

$\dot{()}$ = time derivative

Introduction

SEVERE low-altitude wind variability represents an infrequent but significant hazard to aircraft taking off or landing. During the period from 1964 to 1985, microburst wind shear was a contributing factor in at least 26 civil aviation accidents involving nearly 500 fatalities and over 200 injuries.[1] A microburst is a strong localized downdraft that strikes the ground, creating winds that diverge radially from the impact point. The effects of wind shear on airplane dynamics have only recently been understood in detail, and it has been found that effective recovery from inadvertent encounters may require counterintuitive piloting techniques.[2]

The aviation community has initiated an extensive research effort to solve the wind shear problem. The Federal Aviation Administration (FAA) and NASA have established an integrated program to address the wind shear problem through focused research and development programs.[3,4] The FAA's *Wind Shear Training Aid*[5] recommends that, on recognizing an encounter with severe wind shear, the pilot should command maximum thrust and rotate the aircraft to an initial target pitch angle of 15 deg. This pitch target was identified through rigorous analyses using full six-degree-of-freedom flight simulators and wind models representative of actual accident cases.[6]

The goal of this research is to bridge the gap between the performance achieved using optimal trajectory analysis (OTA) and that attainable using feedback control based on local (and possibly forward-looking) wind field knowledge. OTA permits the determination of aircraft performance limits in wind shear and the control strategies required to achieve such performance.[7–12] Computing these trajectories is an iterative, time-consuming process requiring global wind field knowledge. Because optimal trajectories cannot yet be generated in real time, OTA results are not immediately useful for aircraft control. Feedback control laws employing local wind field knowledge have thus been developed for near-optimal flight control.[13–15]

In a recent paper[16] we presented an optimization study for jet transport encounters with microburst wind shear on final approach. The objective was to execute an escape maneuver that maintained safe ground clearance and an adequate stall margin during the climb-out. A quadratic cost function penalizing deviations in climb rate from a positive nominal value and elevator deflection rate produced qualitatively good escape trajectories. A minimum-airspeed constraint prevented excessive airspeed loss in severe microbursts. The essential feature of the optimal trajectories was that they exchanged altitude for airspeed as a function of microburst strength: in weak to moderate microbursts, the aircraft smoothly shifted from a descent to an ascent at a target climb rate. In severe microbursts,

Received March 1, 1994; revision received Dec. 24, 1994; accepted for publication Dec. 28, 1994.

*Currently Senior Scientist, Charles River Analytics Inc., Cambridge, MA. Member AIAA.

†Professor, Department of Mechanical and Aerospace Engineering. Associate Fellow AIAA.

the aircraft descended through some or all of the core region to prevent excessive airspeed loss.

Although these results provided a qualitative picture of the nature of optimal control in a microburst, they were not immediately applicable to real-time implementation. This paper presents control logic that approximates the performance realized in the optimal trajectories. Given flight-path and speed commands in a wind shear environment, the control law generates appropriate throttle and elevator commands. The controller is designed using the methods of nonlinear inverse dynamics (NID) and time-scale decomposition.[17–23] An airspeed/groundspeed/climb rate guidance scheme developed by Psiaki and Park[24] together with a climb rate scheduling strategy[2] produces trajectories in approach microburst encounters that capture the essence of the optimal trajectories: Altitude is exchanged for airspeed as a function of microburst strength. This result is used in the proposed NID control laws.

Effect of Wind Shear on Airplane Dynamics: Aircraft Model and Equations of Motion

A three-degree-of-freedom model of a twin-jet transport aircraft is used for this study. The aircraft's gross weight is 85,000 lb, and its maximum takeoff thrust is 24,000 lb. Its aerodynamic coefficients are complex nonlinear functions of altitude, Mach number, incidence angles, rotation rates, control deflections, configuration changes (such as gear and flap deflection), and ground proximity. Effects of wind shear on aircraft motion and aerodynamics are modeled as described in Refs. 25 and 26. The relevant reference frames used to describe the aircraft's position, orientation, and velocity are presented in Fig. 1. Flight is assumed to take place in a vertical plane over a flat Earth, and a coordinate system fixed to the ground is defined as the inertial reference frame. On the basis of these assumptions, the equations of motion are

$$\dot{x} = V_a \cos\gamma_a + w_x \tag{1}$$

$$\dot{h} = V_a \sin\gamma_a + w_h \tag{2}$$

$$\dot{V}_a = \frac{T}{m}\cos\alpha_a - \frac{D}{m} - g\sin\gamma_a - \dot{w}_x\cos\gamma_a - \dot{w}_h\sin\gamma_a \tag{3}$$

$$\dot{\gamma}_a = \frac{1}{V_a}\left(\frac{T}{m}\sin\alpha_a + \frac{L}{m} - g\cos\gamma_a - \dot{w}_h\cos\gamma_a + \dot{w}_x\sin\gamma_a\right) \tag{4}$$

$$\dot{\alpha}_a = q - \dot{\gamma}_a \tag{5}$$

$$I_{yy}\dot{q} = M \tag{6}$$

The effect of wind shear on airplane energy state can be described compactly. First define the specific energy (energy per unit weight) as the sum of air mass relative kinetic energy and inertial potential energy:

$$E_s = \left(V_a^2/2g\right) + h \tag{7}$$

Differentiating this expression and substituting from Eqs. (1–3) yield

$$\dot{E}_s = V_a\left(\frac{T\cos\alpha_a - D}{W} - \frac{\dot{w}_x}{g}\cos\gamma_a - \frac{\dot{w}_h}{g}\sin\gamma_a + \frac{w_h}{V_a}\right) \tag{8}$$

The first term is recognizable as the airplane's specific excess power. The three wind terms describe wind shear impact on airplane energy state, and they may be combined into a single scalar quantity called the F factor[3] as follows:

$$F = \frac{\dot{w}_x}{g}\cos\gamma_a + \frac{\dot{w}_h}{g}\sin\gamma_a - \frac{w_h}{V_a} \tag{9}$$

The vertical shear term is typically quite small and often neglected. The effect of wind shear on airplane performance is thus expressed as an effective reduction in available specific excess power due to horizontal and vertical shears and downdrafts. Regions where F is negative are performance-increasing shears, whereas those where F is positive are performance decreasing. The F values of more than 0.15 cancel the climb gradient capability of most jet transports.

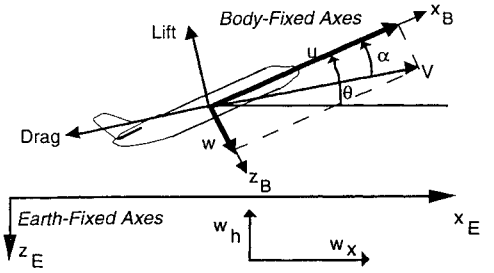

Fig. 1 Coordinate system and reference frames.

The longitudinal equations of motion can be expressed using inertial-axis variables as well. First define the difference between inertial and air-relative angle of attack as

$$\Delta\alpha = \alpha_i - \alpha_a \tag{10}$$

Then, the equations of motion become

$$\dot{x} = V_i\cos\gamma_i \tag{11}$$

$$\dot{h} = V_i\sin\gamma_i \tag{12}$$

$$\dot{V}_i = \frac{T}{m}\cos\alpha_i - \frac{D}{m}\cos(\Delta\alpha) - \frac{L}{m}\sin(\Delta\alpha) - g\sin\gamma_i \tag{13}$$

$$\dot{\gamma}_i = \frac{1}{V_i}\left(\frac{T}{m}\sin\alpha_i + \frac{L}{m}\cos(\Delta\alpha) - \frac{D}{m}\sin(\Delta\alpha) - g\cos\gamma_i\right) \tag{14}$$

$$\dot{\alpha}_i = q - \dot{\gamma}_i \tag{15}$$

The pitch acceleration is defined as in Eq. (6). Lift, drag, pitching moment, and thrust are expressed as

$$L = \bar{q}S_{\text{ref}}C_L \tag{16}$$

$$D = \bar{q}S_{\text{ref}}C_D \tag{17}$$

$$T = T_{\max}(V_a)\delta_T \qquad 0 \le \delta_T \le 1 \tag{18}$$

$$M = \bar{q}S_{\text{ref}}\bar{c}C_M \tag{19}$$

The wind components and spatial gradients used in the equations of motion are obtained from the Oseguera–Bowles downburst model.[27] This analytic time-invariant model represents an axisymmetric stagnation point flow, and it permits simulation of microbursts of varying size and strength through specification of the radius of the downdraft column, the maximum outflow, and the altitude of maximum outflow.

Nonlinear Flight Control

This description of nonlinear control methods is necessarily brief. More complete treatments can be found in Refs. 28 and 29. The following derivation is from Ref. 30. Given a system of the form

$$\dot{\boldsymbol{x}} = \boldsymbol{f}(\boldsymbol{x}) + \boldsymbol{G}(\boldsymbol{x})\boldsymbol{u} \tag{20}$$

where $\boldsymbol{x}$ is $n \times 1$ and $\boldsymbol{u}$ is $m \times 1$, we define an m-dimensional output vector

$$\boldsymbol{y} = \boldsymbol{H}(\boldsymbol{x}) \tag{21}$$

It is possible to define a nonlinear feedback control law that provides output decoupling of the elements of $\boldsymbol{y}$ or their derivatives such that $\boldsymbol{y}^{(d)} = \boldsymbol{v}$. The new control input $\boldsymbol{v}$ can be chosen to place the system poles in desired locations (for example, to achieve desired specifications on response overshoot and settling time). The vector $\boldsymbol{y}^{(d)}$ is expressed as

$$\boldsymbol{y}^{(d)} = \boldsymbol{f}^*(\boldsymbol{x}) + \boldsymbol{G}^*(\boldsymbol{x})\boldsymbol{u} = \boldsymbol{v} \tag{22}$$

where d is the relative degree of differentiation required to identify a direct control effect on each element of the output vector. The inverse control law then takes the form

$$\boldsymbol{u} = [\boldsymbol{G}^*(\boldsymbol{x})]^{-1}[\nu - \boldsymbol{f}^*(\boldsymbol{x})] \tag{23}$$

and the closed-loop dynamics of the system are

$$\dot{\boldsymbol{x}} = \boldsymbol{f}(\boldsymbol{x}) + \boldsymbol{G}(\boldsymbol{x})[\boldsymbol{G}^*(\boldsymbol{x})]^{-1}[\nu - \boldsymbol{f}^*(\boldsymbol{x})] \tag{24}$$

While the expression of the inverse control law appears simple, its implementation can be quite complex. Evaluation of the functions $\boldsymbol{f}^*(\boldsymbol{x})$ and $\boldsymbol{G}^*(\boldsymbol{x})$ requires that a full, d-differentiable model of the aircraft dynamics be included in the control system. The controller can be simplified if the system can be partitioned into slow- and fast-time-scale subsystems.[31] The separation of the dynamics into fast and slow time scales is a natural consequence of the underlying physics. For the aircraft problem, it is assumed that the pitch rate evolves faster than the flight path and velocity. This is consistent with the time-scale separation between the phugoid and short-period modes of an aircraft's longitudinal dynamics.[32] This technique has been applied to the flight control problem.[19–23] The present study departs from previous applications of NID to flight control in that the effects of wind shear are explicitly considered in the inversion.

Controller Design

Inertial Speed/Climb Rate Control Mode

The objective is to control climb rate and inertial speed by sequentially inverting the aircraft dynamic equations. The output vector is

$$\boldsymbol{y}(t) = \begin{bmatrix} \dot{h}(t) \\ V_i(t) \end{bmatrix} \tag{25}$$

The controller is partitioned into an outer loop and an inner loop. The control commands generated by the outer loop are pitch rate q_c and commanded engine thrust T_c. Although aircraft lift does depend on δ_E, the effect is small and is not a primary path of aerodynamic control. It has been shown[33] that inverse control laws exploiting such weak aerodynamic effects either generate unreasonably large control deflections in response to small state perturbations or destabilize the system by canceling the nonlinear equivalent of non-minimum-phase transmission zeros. Thus for the present design, δ_E contribution to lift is included when L is calculated in the simulation, but the controller does not exploit the effect.

The engine dynamics are modeled as a first-order lag:

$$\dot{T} = \frac{1}{\tau}(T_c - T) \tag{26}$$

The time constant τ is set to 2 s. The inverse controller is developed by differentiating Eq. (25) twice, so that the controls T_c and q_c appear linearly. Although L and D are, in principle, dependent on q, its contribution is very small and an inverse controller exploiting this unsteady aerodynamic effect would command very large pitch rates in response to small state perturbations. When lift and drag are calculated for simulation, pitch rate effects are included. However, the inverse controller is derived as though pitch rate has no effect on lift or drag. To complete the inversion, time rates of change of lift and drag are expressed as

$$\dot{L} \equiv E_1 + E_2 q_c \tag{27}$$

$$\dot{D} \equiv F_1 + F_2 q_c \tag{28}$$

with the pitch rate q_c treated as a control input. The expressions for E_1 and E_2 are developed by differentiating the aircraft's aerodynamic coefficients with respect to time. Differentiating Eq. (25) twice and substituting from Eqs. (10–15), one obtains

$$\ddot{\boldsymbol{y}} = \boldsymbol{f}_I^* + \boldsymbol{G}_I^* \boldsymbol{u} = \nu \tag{29}$$

where

$$\boldsymbol{f}_I^* = \begin{bmatrix} f_1 \\ f_2 \end{bmatrix} \quad \boldsymbol{G}_I^* = \begin{bmatrix} g_{11} & g_{12} \\ g_{21} & g_{22} \end{bmatrix} \quad \boldsymbol{u} = \begin{bmatrix} T_c \\ q_c \end{bmatrix} \quad \nu = \begin{bmatrix} \nu_1 \\ \nu_2 \end{bmatrix} \tag{30}$$

The f_i and g_{ij} are determined by differentiating the original motion equations:

$$f_1 = -\frac{F_1}{m}\sin\gamma_a - \frac{T}{m\tau}\sin\theta - \frac{D}{m}\dot{\gamma}_a\cos\gamma_a + \frac{E_1}{m}\cos\gamma_a - \frac{L}{m}\dot{\gamma}_a\sin\gamma_a \tag{31}$$

$$f_2 = -\frac{T}{m\tau}\cos\alpha_i + \frac{T}{m}\dot{\gamma}_i\sin\alpha_i - \frac{F_1}{m}\cos(\alpha_i - \alpha_a) + \frac{D}{m} \times (\dot{\alpha}_i - \dot{\alpha}_a)\sin(\alpha_i - \alpha_a) - \frac{E_1}{m}\sin(\alpha_i - \alpha_a) - \frac{L}{m}(\dot{\alpha}_i - \dot{\alpha}_a) \times \cos(\alpha_i - \alpha_a) - g\dot{\gamma}_i\cos\gamma_i \tag{32}$$

$$g_{11} = \frac{1}{m\tau}\sin\theta \tag{33}$$

$$g_{12} = \frac{T}{m}\cos\theta - \frac{F_2}{m}\sin\gamma_a + \frac{E_2}{m}\cos\gamma_a \tag{34}$$

$$g_{21} = \frac{1}{m\tau}\cos\alpha_i \tag{35}$$

$$g_{22} = -\frac{T}{m}\sin\alpha_i - \frac{F_2}{m}\cos(\alpha_i - \alpha_a) - \frac{E_2}{m}\sin(\alpha_i - \alpha_a) \tag{36}$$

Rearranging Eq. (29) yields

$$\boldsymbol{u} = [\boldsymbol{G}_I^*]^{-1}(\nu - \boldsymbol{f}_I^*) \tag{37}$$

It remains to determine the nature of the new control input ν and the means by which the desired pitch rate q_c is achieved.

Desired Outer Loop Dynamics

The form of the control inputs ν_1 and ν_2 must be specified. Presently, proportional-integral-derivative (PID) control is used. Thus,

$$\ddot{h}(t) = \nu_1 = k_1[\dot{h}_{\text{com}}(t) - \dot{h}(t)] - k_2\ddot{h}(t) + k_3 \times \int_{t_0}^{t}[\dot{h}_{\text{com}}(\tau) - \dot{h}(\tau)]\,\mathrm{d}\tau \tag{38}$$

$$\ddot{V}_i(t) = \nu_2 = k_4\left[V_{i_{\text{com}}}(t) - V_i(t)\right] - k_5\dot{V}_i(t) + k_6 \times \int_{t_0}^{t}\left[V_{i_{\text{com}}}(\tau) - V_i(\tau)\right]\mathrm{d}\tau \tag{39}$$

where $\dot{h}_{\text{com}}$ and V_{com} are the commanded altitude rate and inertial speed, respectively. Define $r(t)$ as

$$r(t) \equiv \dot{h}(t) \tag{40}$$

Substituting Eq. (40) into Eq. (38) and taking the Laplace transforms of Eq. (38) and (39), yield

$$r(s) = \frac{k_1 s + k_3}{s^3 + k_2 s^2 + k_1 s + k_3} r_{\text{com}}(s) \tag{41}$$

$$V_i(s) = \frac{k_4 s + k_6}{s^3 + k_5 s^2 + k_4 s + k_6} V_{i_{\text{com}}}(s) \tag{42}$$

By choosing the gains k_i appropriately, the outer loop response of the aircraft can be shaped as desired. The nonlinear dynamics of the aircraft are thus transformed into those of a pair of third-order linear systems using the technique described here. The method used to achieve the commanded pitch rate q_c is now described.

Inner Loop Dynamics

The inner loop control law generates the pitch rate q_c commanded by the outer loop controller. We define

$$\Delta q(t) \equiv q(t) - q_c(t) \tag{43}$$

The inner loop controller regulates Δq to zero. For the aircraft to respond to speed or climb rate commands with the dynamics of

Eqs. (41) and (42), the inner loop controller must generate the required pitch rate on a time scale much shorter than that of the outer loop dynamics. As a practical matter, the inner loop dynamics should be chosen to have a time constant that is at least 3–5 times faster than the outer loop. The inner loop dynamics take the form

$$\Delta\dot{q} = \nu_3 = -k_7 \Delta q \tag{44}$$

If the time scales of the two controllers are sufficiently separated, on the inner loop time scale, $q_c \approx 0$. Assuming this approximation to be an equality,

$$\dot{q} + k_7 q = k_7 q_c \tag{45}$$

Taking the Laplace transform of this expression,

$$q(s) = \frac{k_7}{s + k_7} q_c(s) \tag{46}$$

The constant k_7 can be chosen to achieve a sufficiently fast response. The validity of this technique depends on adequate time-scale separation between the inner and outer loop dynamics.[34] Elevator bandwidth limits place a constraint on the time constant achievable in Eq. (46). The necessary elevator deflection is calculated by inverting the pitch rate dynamics. From Eqs. (6) and (19),

$$\dot{q} = \frac{\bar{q} S_{\text{ref}} \bar{c}}{I_{yy}} C_M \tag{47}$$

The pitching moment can be written as

$$C_M = C_{M_0}(h,\ V_a,\ \alpha,\ \dot{\alpha},\ q,\ \delta_T) + C_{M_{\delta_E}} \delta_E \tag{48}$$

Combining Eqs. (44), (47), and (49) yields

$$\delta_E = \frac{1}{C_{M_{\delta_E}}} \left[\frac{I_{yy} \nu_3}{\bar{q} S_{\text{ref}} \bar{c}} - C_{M_0} \right] \tag{49}$$

The inertial speed/climb rate controller development is thus complete. The airspeed/climb rate controller is now presented.

Airspeed/Climb Rate Control Mode

In this mode, the objective is to regulate airspeed and climb rate about nominal values. The output vector is

$$y(t) = \begin{bmatrix} \dot{h}(t) \\ V_a(t) \end{bmatrix} \tag{50}$$

As before, the output is differentiated twice. We thus obtain

$$\ddot{\mathbf{y}} = \boldsymbol{f}_A^* + \boldsymbol{G}_A^* \boldsymbol{u} = \boldsymbol{\nu} \tag{51}$$

where

$$\boldsymbol{f}_A^* = \begin{bmatrix} a_1 \\ a_2 \end{bmatrix} \qquad \boldsymbol{G}_A^* = \begin{bmatrix} b_{11} & b_{12} \\ b_{21} & b_{22} \end{bmatrix}$$
$$\boldsymbol{u} = \begin{bmatrix} T_c \\ q_c \end{bmatrix} \qquad \boldsymbol{\nu} = \begin{bmatrix} \nu_4 \\ \nu_5 \end{bmatrix} \tag{52}$$

Using the terms defined in Eqs. (31–36),

$$a_1 = f_1 \tag{53}$$

$$a_2 = -\frac{T}{m\tau} \cos\alpha_a + \frac{T}{m} \dot{\gamma}_a \sin\alpha_a - \frac{F_1}{m} - g\dot{\gamma}_a \cos\gamma_a + \dot{w}_x \dot{\gamma}_a \sin\gamma_a - \dot{w}_h \dot{\gamma}_a \cos\gamma_a - \ddot{w}_x \cos\gamma_a - \ddot{w}_h \sin\gamma_a \tag{54}$$

$$b_{11} = g_{11} \tag{55}$$

$$b_{12} = g_{12} \tag{56}$$

$$b_{21} = \frac{1}{m\tau} \cos\alpha_a \tag{57}$$

$$b_{22} = -\frac{T}{m} \sin\alpha_a - \frac{F_2}{m} \tag{58}$$

Rearranging Eq. (52) yields the control input $\boldsymbol{u}$:

$$\boldsymbol{u} = [\boldsymbol{G}_A^*]^{-1} (\boldsymbol{\nu} - \boldsymbol{f}_A^*) \tag{59}$$

Several wind component time derivatives are needed in the calculation of a_2. They are computed using spatial derivatives obtained directly from the Oseguera–Bowles model. In practice, it would be necessary to estimate the wind derivatives from available inertial and air data measurements. For this preliminary study, it is assumed that they are known exactly. A later study[35] addresses the estimation of these components.

The form of the outer loop dynamics of the airspeed/climb rate controller is identical to that of the inertial speed/climb rate controller and is not described further. The same inner loop dynamics are used for both the groundspeed and airspeed controllers.

Control Issues in Microburst Environment

In a classical microburst, the aircraft typically first encounters a performance-increasing headwind. If airspeed is regulated about a nominal value, a reduction in thrust would be commanded, leaving the aircraft in a precarious situation once the headwind is replaced by a performance-decreasing downdraft and tailwind. As such, airspeed should not be regulated blindly by a microburst. Inertial-speed control, subject to a minimum-airspeed constraint, might be desirable during a final approach in a microburst.[36] Control of inertial speed prevents too high a touchdown velocity, whereas the minimum-airspeed constraint maintains an adequate stall margin in the convective wind shear environment. During takeoff or an aborted landing, airspeed control is a concern, since the airplane's ability to climb or maintain altitude depends on its speed with respect to the local air mass. A conservative strategy during an escape would be to command full throttle. The control law should be structured so that it does not command an inadvertent thrust reduction in the microburst's performance-increasing area. One possible solution is to regulate the minimum of airspeed and groundspeed to a nominal value,[24] as discussed below. In an escape maneuver, full throttle and a desired climb rate can be commanded, so that the aircraft's full performance capability is used as soon as possible.

Groundspeed/Airspeed Control Law

In Ref. 24, Psiaki and Park present a throttle control law that regulates the minimum of airspeed and groundspeed to a nominal value in a microburst environment. The same nominal value is set for both airspeed and groundspeed, and a thrust feedback loop regulates the minimum of the two speeds to this nominal value. In still air, airspeed and groundspeed are identical, and the control law behaves like an airspeed controller. In a microburst's performance-increasing area, groundspeed is less than airspeed, and a reduction in thrust is not commanded. In the tailwind area, airspeed is the minimum of the two speeds, and thrust is increased while the aircraft is in a performance-decreasing shear. This control structure is extended here into a throttle/pitch control law for flight-path tracking in wind shear.

The controller structure is developed by rewriting Eqs. (29) and (51) as

$$\ddot{\boldsymbol{y}}_I = \boldsymbol{f}_I^* + \boldsymbol{G}_I^* \boldsymbol{u}_I = \boldsymbol{\nu}_I \tag{60}$$

$$\ddot{\boldsymbol{y}}_A = \boldsymbol{f}_A^* + \boldsymbol{G}_A^* \boldsymbol{u}_A = \boldsymbol{\nu}_A \tag{61}$$

The additional subscripts I and A are introduced to distinguish control inputs generated by the groundspeed/climb rate and airspeed/climb rate controllers, respectively. The same nominal value is used for the commanded airspeed and groundspeed for the purposes of calculating the elements of $\boldsymbol{\nu}_I$ and $\boldsymbol{\nu}_A$. During a microburst encounter, the aircraft responds with the dynamics of either Eq. (61) or (62), depending on the relative magnitude of T_c and T_{c_A}. If $T_{c_I} > T_{c_A}$, then $T_c = T_{c_I}$ and $q_c = q_{c_I}$. Conversely if $T_{c_A} > T_{c_I}$, then $T_c = T_{c_A}$ and $q_c = q_{c_A}$. In other words, the throttle setting and commanded pitch rate depend on the relative magnitude of the thrust commands generated by the airspeed/climb rate controller and the groundspeed/climb rate controller.

In the event of throttle saturation, complete output variable independence cannot be maintained. Saturation injects discontinuities into the system, and the resultant response may not look anything like the desired dynamics.[33] However, partial independence can be maintained by dropping one of the command variables from the command set and including the saturation effect into the calculation of the inverse dynamics of the remaining command variable.[18] Presently, the controller maintains climb rate tracking in the event of throttle saturation. It recovers full command variable independence once the commanded thrust drops below the maximum available. In order to prevent transient stall, an extension to the slack-variable technique for trajectory optimization[37] developed by Zhao and Bryson[13] is used to enforce an upper limit on the aircraft's angle of attack.

During an aborted-landing maneuver, the command vector is

$$y_{\text{escape}}(t) = \begin{bmatrix} T(t) \\ \dot{h}(t) \end{bmatrix} \tag{62}$$

This output vector is slightly different from the previous two. The time derivative of T is a function only of T and the commanded thrust T_c [Eq. (26)]. No number of differentiations of the first element will bring out a dependence on q. Since a first-order model of thrust dynamics is assumed, T is differentiated once to make T_c appear linearly. The second element is differentiated twice as before. The resultant dynamics have the form

$$\begin{bmatrix} \dot{T}(t) \\ \ddot{h}(t) \end{bmatrix} = \begin{bmatrix} v_6 \\ v_7 \end{bmatrix} \tag{63}$$

During an aborted-landing maneuver, full throttle and a desired climb rate are commanded.

Climb Rate Scheduling

The trajectories developed in Ref. 16 show that an optimal guidance strategy during aborted-landing maneuvers in wind shear is to schedule climb rate as a function of microburst strength: in weak-to-moderate microbursts, the aircraft smoothly shifts from a descent on the glide slope to an ascent at the target climb rate; in severe microbursts, the aircraft descends through some or all of the core region to prevent excessive airspeed loss. These results were obtained through the iterative process of trajectory optimization. The question arises of how to capture the essence of this strategy for the purposes of real-time control.

In Ref. 2, Hinton compares the performance of several different flight management strategies for escape from microburst encounters during takeoff. The most effective strategy (in terms of minimum recovery altitudes and insensitivity to shear strength) is found to be one that schedules the target climb rate as a function of the potential climb rate (which depends on airspeed and F). Assuming negligible energy loss when trading airspeed for climb rate, the potential climb rate $\dot{h}_p$ is equal to the rate of change of total specific energy [Eq. (7)] and is given by

$$\dot{h}_p = \dot{E}_s = \frac{V_a \dot{V}_a}{g} + \dot{h} \tag{64}$$

This quantity can be measured directly using existing total-energy sensors.[38] Potential climb rate is related to the potential flight-path angle γ_{i_p} through the relation

$$\dot{h}_p = V_i \sin \gamma_{i_p} \tag{65}$$

Hinton proposed a flight management strategy that, above a certain safe altitude, targeted a climb if γ_{i_p} was positive (implying weak or no shear) and targeted a flight-path angle of $k\gamma_{i_p}$ if γ_{i_p} was negative (implying a strong shear). The gain k could be varied from 0 (commanding level flight) to 1 (commanding a constant-airspeed descent). Highest recovery altitudes were produced using $k = 0.5$ for microburst encounters during takeoff.

Table 1 NID feedback gains

Gain	Value
k_1, k_4	$0.7416\ \text{s}^{-2}$
k_2, k_5	$1.2185\ \text{s}^{-1}$
k_3, k_6	$0.16\ \text{s}^{-3}$
k_7	$5.0\ \text{s}^{-1}$

Table 2 Microburst parameter sets for control law evaluation

Microburst no.	R, ft	$U_{\max}$, ft/s	$z_{\max}$, ft
1	3000	60	150
2	3000	70	150
3	3000	80	150
4	3000	90	150
5	3000	100	150
6	3000	110	150

This strategy is adopted here for the purpose of determining the target climb rate $\dot{h}_{\text{com}}$ during an aborted-landing maneuver in wind shear. The commanded climb rate is defined as

$$\dot{h}_{\text{com}} = \begin{cases} 5 & \dot{h}_p > 5 \text{ ft/s} \\ \dot{h}_p & 0 \le \dot{h}_p \le 5 \\ k\dot{h}_p & \dot{h}_p < 0 \end{cases} \tag{66}$$

In effect, this strategy schedules climb rate as a function of the aircraft's instantaneous available climb performance. The gain k is set to 0.1 for the results that follow.

Controller Evaluation

The nonlinear control laws are evaluated for microburst encounters on the final approach. The aircraft tracks a reference descent rate using the groundspeed/airspeed control law discussed in the preceding section. An aborted-landing maneuver is commanded using full throttle and a reference climb rate of 5 ft/s once F [Eq. (9)] exceeds an alert threshold of 0.075. The controller gains are listed in Table 1. Flight is considered through several different microbursts, and Table 2 lists their parameter sets. The aircraft is initialized on the glide slope 7500 ft away from the microburst core at an altitude of 975 ft, with a groundspeed of 245 ft/s. The nominal airspeed and groundspeed used in the control laws are both equal to this initial groundspeed.

Simulations are conducted both with and without the climb rate scheduling technique. Figures 2–5 present state and control histories for the trajectories computed without climb rate scheduling. Figure 6 shows the wind shear F factor experienced through each of the microbursts. Figures 7–10 present the state and control histories obtained using climb rate scheduling. The associated F factor curves are omitted in the interest of brevity.

Without climb rate scheduling (i.e., with a constant target climb rate), the aircraft tracks the target climb rate of 5 ft/s in all the two most severe microbursts (5 and 6). In microburst 5, the aircraft departs slightly from the target climb rate of 5 ft/s for a brief period in the tailwind region. In microburst 6, the aircraft flies at its maximum angle of attack for approximately 3000 ft (above 14 s). The aircraft departs rapidly and severely from the 5 ft/s climb rate, descending to an altitude of about 400 ft before starting to climb again. The airspeed drops precipitously low (the aircraft's 1-g stall speed is approximately 150 ft/s in the approach configuration), and the aircraft undergoes sharp angle-of-attack transients. The peak F experienced by the aircraft ranges from 0.25 in microburst 1 to 0.45 in microburst 6. Since the climb capability of typical jet transports is canceled by persistent F values greater than 0.15, these simulated microbursts are good candidates for evaluating controller performance. In all microbursts, throttle setting increases during the glide-slope tracking portion of the trajectory in order to maintain groundspeed.

The features of the flight paths through the most severe microburst suggest that the "open-loop" strategy of targeting a constant climb

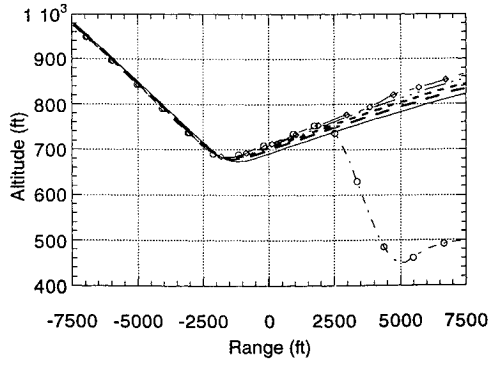

Fig. 2 Altitude vs range. — U_{max} = 60 ft/s, – – – U_{max} = 70 ft/s, - - - - U_{max} = 80 ft/s, — - - - - U_{max} = 90 ft/s, —◇ - - U_{max} = 100 ft/s, – - ⊖ - - U_{max} = 110 ft/s.

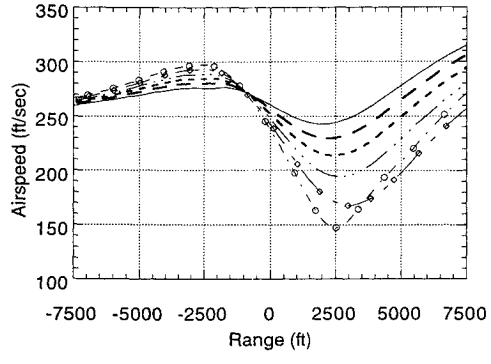

Fig. 3 Airspeed vs range. — U_{max} = 60 ft/s, – – – U_{max} = 70 ft/s, - - - - U_{max} = 80 ft/s, — - - - - U_{max} = 90 ft/s, —◇ - - U_{max} = 100 ft/s, – - ⊖ - - U_{max} = 110 ft/s.

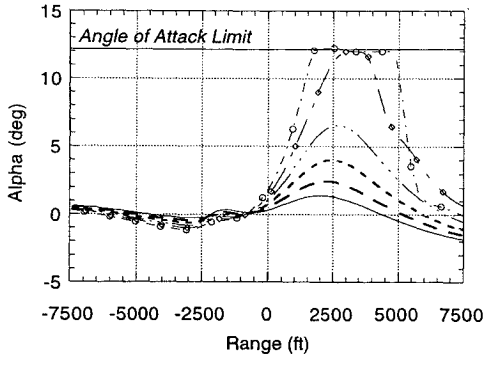

Fig. 4 Angle of attack vs range. — U_{max} = 60 ft/s, – – – U_{max} = 70 ft/s, - - - - U_{max} = 80 ft/s, — - - - - U_{max} = 90 ft/s, —◇ - - U_{max} = 100 ft/s, – - ⊖ - - U_{max} = 110 ft/s.

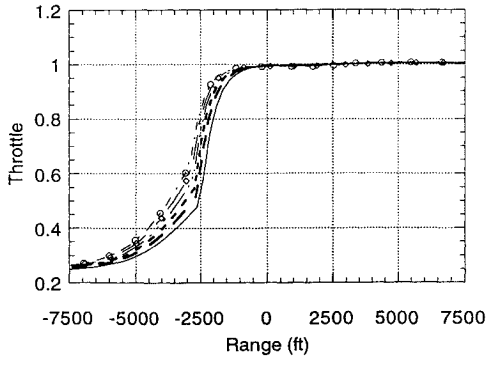

Fig. 5 Throttle vs range. — U_{max} = 60 ft/s, – – – U_{max} = 70 ft/s, - - - - U_{max} = 80 ft/s, — - - - - U_{max} = 90 ft/s, —◇ - - U_{max} = 100 ft/s, – - ⊖ - - U_{max} = 110 ft/s.

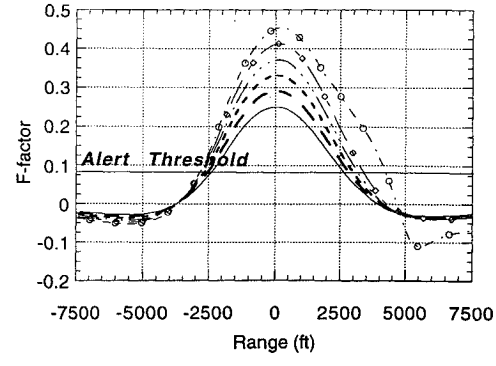

Fig. 6 The *F* factor vs range. — U_{max} = 60 ft/s, – – – U_{max} = 70 ft/s, - - - - U_{max} = 80 ft/s, — - - - - U_{max} = 90 ft/s, —◇ - - U_{max} = 100 ft/s, – - ⊖ - - U_{max} = 110 ft/s.

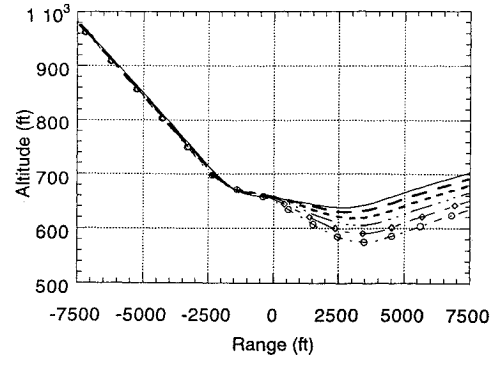

Fig. 7 Altitude vs range with climb rate scheduling. — U_{max} = 60 ft/s, – – – U_{max} = 70 ft/s, - - - - U_{max} = 80 ft/s, — - - - - U_{max} = 90 ft/s, —◇ - - U_{max} = 100 ft/s, – - ⊖ - - U_{max} = 110 ft/s.

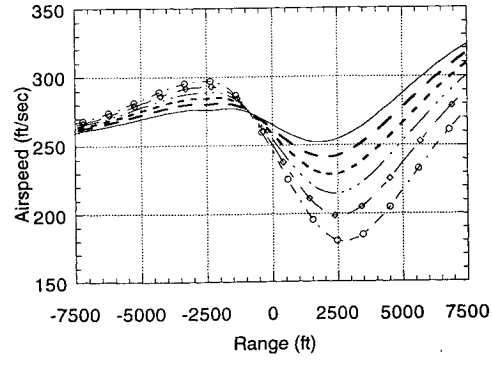

Fig. 8 Airspeed vs range with climb rate scheduling. — U_{max} = 60 ft/s, – – – U_{max} = 70 ft/s, - - - - U_{max} = 80 ft/s, — - - - - U_{max} = 90 ft/s, —◇ - - U_{max} = 100 ft/s, – - ⊖ - - U_{max} = 110 ft/s.

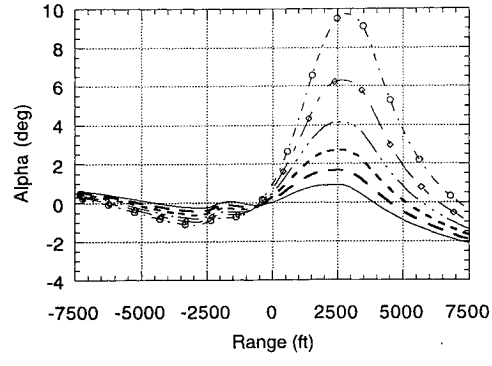

Fig. 9 Angle of attack vs range with climb rate scheduling. — U_{max} = 60 ft/s, – – – U_{max} = 70 ft/s, - - - - U_{max} = 80 ft/s, — - - - - U_{max} = 90 ft/s, —◇ - - U_{max} = 100 ft/s, – - ⊖ - - U_{max} = 110 ft/s.

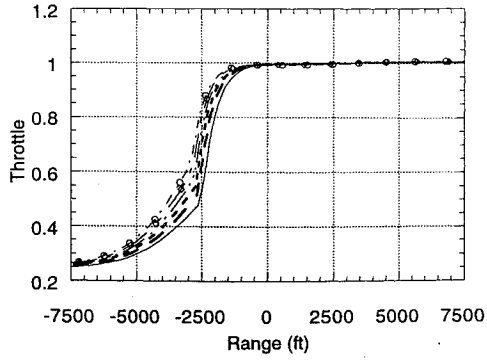

Fig. 10 Throttle vs range with climb rate scheduling. — U_{max} = 60 ft/s, – – – U_{max} = 70 ft/s, - - - - - U_{max} = 80 ft/s, — - - - - U_{max} = 90 ft/s, —◇ - - U_{max} = 100 ft/s, – - ⊖ - - U_{max} = 110 ft/s.

rate during an aborted landing has serious shortcomings. Although most real-world microbursts are less intense (i.e., lower F) than the ones considered, the simulation results suggest that the constant-climb-rate strategy could allow the aircraft to descend into the ground in the most critical situations. This situation is remedied by climb rate scheduling (Figs. 7–10), which produces markedly different altitude profiles. Without climb rate scheduling, the aircraft immediately transitions from descending to ascending flight in all six microbursts. With climb rate scheduling, all of the flight paths become shallow descents through the core region. Figure 7 shows that the aircraft descends more with increasing microburst strength. The aircraft transits each of the microbursts with generally higher airspeeds in Fig. 8 than it does in Fig. 3. Correspondingly, much lower angles of attack are experienced in Fig. 9 than in Fig. 3.

The simulation results show that NID control laws with climb rate scheduling can make effective use of aircraft performance and local wind knowledge to safely transit a very severe microburst. The resultant flight paths are qualitatively similar to the optimal trajectories in Ref. 16 in that a trade-off is created between airspeed and altitude. The degree of this trade-off may be altered by changing the gain k in Eq. (67). The gain also could be made a function of altitude, so that the aircraft is forced to climb if it is below some minimum safe altitude.

Recent work has assessed the robustness of the controller to uncertainty in the aerodynamic model, and it considered the issue of estimating the aircraft state from the sensor outputs available on a typical jet transport.[35] It has been found that an extended Kalman filter (EKF) can produce accurate estimates of the aircraft state and disturbance inputs. In particular, the EKF can estimate wind components and their time derivatives with sufficient accuracy that trajectories produced by driving the NID control laws with the state and disturbance estimates closely match those obtained using perfect state feedback. Uncertainty in plant dynamics is handled effectively by treating it as a fictitious disturbance input[39] in the EKF equations.

Conclusions

A wind shear flight control law based on sequential inversion of longitudinal aircraft dynamics has been presented. Time-scale decomposition partitions in the aircraft's dynamics into fast and slow subsystems, and inverting control laws are developed for each subsystem. The approach control logic uses a combination of groundspeed/airspeed and climb rate control. During aborted-landing encounters, the command variables are throttle setting and climb rate. The combination of groundspeed and airspeed control overcomes the shortcomings of either airspeed or groundspeed control. Direct control of thrust permits application of the maximum available thrust during the aborted-landing maneuver. A climb rate scheduling strategy trades off altitude for airspeed as a function of microburst strength, attenuating excessive airspeed loss in very severe microbursts. The simulation results suggest that with properly designed control laws, the jet transport considered in this study can safely transit very severe microbursts. It is concluded that the NID control laws are good candidates for operational implementation.

References

[1]Townsend, J., *Low-Altitude Wind Shear and Its Hazard to Aviation*, National Academy, Washington, DC, 1983.

[2]Hinton, D. A., "Flight Management Strategies for Escape from Microburst Encounters," NASA TM-4057, Aug. 1988.

[3]Bowles, R. L., "Reducing Windshear Risk Through Airborne Systems Technology," presented at the 17th Congress of the Intl. Council of the Aeronautical Sciences, Stockholm, Sweden, Sept. 1990.

[4]Hinton, D. A., "Piloted-Simulation Evaluation of Recovery Guidance for Microburst Wind Shear Encounters," NASA TP 2886, March 1989.

[5]*Windshear Training Aid*, U.S. Department of Transportation, Federal Aviation Administration, Washington, DC, 1987.

[6]Kupcis, E. A., "Manually Flown Windshear Recovery Technique," *Proceedings of the 29th Conference on Decision and Control*, Honolulu, HI, Dec. 1990, pp. 758, 759.

[7]Miele, A., "Optimal Trajectories and Guidance Trajectories for Aircraft Flight Through Windshears,"*Proceedings of the 29th Conference on Decision and Control*, Honolulu, HI, Dec. 1990, pp. 737–746.

[8]Psiaki, M. L., and Stengel, R. F., "Analysis of Aircraft Control Strategies for Microburst Encounter," *Journal of Guidance, Control, and Dynamics*, Vol. 8, No. 5, 1985, pp. 553–559.

[9]Psiaki, M. L., "Control of Flight Through Microburst Wind Shear Using Deterministic Trajectory Optimization," Ph.D. Dissertation, Princeton Univ., Princeton, NJ, 1987 (Rept. No. 1787-T).

[10]Psiaki, M. L., and Stengel, R. F., "Optimal Aircraft Performance During Microburst Encounter," *Journal of Guidance, Control, and Dynamics*, Vol. 14, No. 2, 1991, pp. 440–446.

[11]Zhao, Y., and Bryson, A. E., "Optimal Paths Through Downbursts," *Journal of Guidance, Control, and Dynamics*, Vol. 13, No. 5, 1990, pp. 813–818.

[12]Mulgund, S. S., and Stengel, R. F., "Target Pitch Angle for the Microburst Escape Maneuver," *Journal of Aircraft*, Vol. 30, No. 6, 1993, pp. 826–832.

[13]Zhao, Y., and Bryson, A. E., "Control of an Aircraft in Downbursts," *Journal of Guidance, Control, and Dynamics*, Vol. 13, No. 5, 1990, pp. 819–823.

[14]Miele, A., Wang, T., and Melvin, W., "Guidance Strategies for Near-Optimum Takeoff Performance in Wind Shear," *Journal of Optimization Theory and Applications*, Vol. 50, No. 1, 1986, pp. 1–47.

[15]Miele, A., Wang, T., and Melvin, W., "Optimization and Gamma/Theta Guidance of Flight Trajectories in a Windshear," presented at the 15th Congress of the Intl. Council of the Aeronautical Sciences, London, Sept. 1986.

[16]Mulgund, S. S., and Stengel, R. F., "Optimal Recovery from Microburst Wind Shear," *Journal of Guidance, Control, and Dynamics*, Vol. 16, No. 6, 1993.

[17]Morton, B. G., Elgersma, M. R., Harvey, C., and Hines, G., "Nonlinear Flying Quality Parameters Based on Dynamic Inversion," Honeywell Systems and Research Center, AFWAL-TR-87-3079, Minneapolis, MN, Oct. 1987.

[18]Lane, S., and Stengel, R. F., "Flight Control Using Non-Linear Inverse Dynamics," *Automatica*, Vol. 24, No. 4, 1988, pp. 471–483.

[19]Menon, P. K., Badgett, M., and Walker, R., "Nonlinear Flight Test Controllers for Aircraft," *Journal of Guidance, Control, and Dynamics*, Vol. 10, No. 1, 1987.

[20]Menon, P. K., Chatterji, G., and Cheng, V., "A Two-Time-Scale Autopilot for High Performance Aircraft," *Proceedings of the 1991 AIAA Guidance, Navigation, and Control Conference* (New Orleans), AIAA, Washington, DC, 1991.

[21]Meyer, G., and Cicolani, L., "Application of Nonlinear System Inverses to Automatic Flight Control Designs: System Concepts and Flight Evaluations," *Theory and Application of Optimal Control in Aerospace Systems*, AGARD, AG251, pp. 10.1–10.29.

[22]Hauser, J., Sastry, S., and Meyer, G., "Nonlinear Control Design for Slightly Non-Minimum Phase Systems: Application to V/STOL Aircraft," *presented at the IFAC Conference NOLCOS '89*, Capri, Italy, June 1989.

[23]Elgersma, M., and Morton, B., "Partial Inversion of Noninvertible Nonlinear Aircraft Models," Honeywell Systems Research Center, Minneapolis, MN, Aug. 1989.

[24]Psiaki, M., and Park, K., "Thrust Laws for Microburst Wind Shear Penetration," *Journal of Guidance, Control, and Dynamics*, Vol. 15, No. 4, 1992, pp. 968–975.

[25]Frost, W., and Bowles, R., "Wind Shear Terms in the Equations of Aircraft Motion," *Journal of Aircraft*, Vol. 21, No. 11, 1984, pp. 866–872.

[26]Stengel, R. F., "Course Notes for MAE 566: Aircraft Dynamics," Princeton Univ., Princeton, NJ, Jan. 1990.

[27]Oseguera, R. M. and Bowles, R. L., "A Simple, Analytic 3-Dimensional Downburst Model Based on Boundary Layer Stagnation Flow," NASA TM-100632, Washington, DC, July 1988.

[28]Singh, S. N., and Rugh, W. J., "Decoupling in a Class of Nonlinear Systems by State Feedback," *ASME Journal of Dynamic Systems, Measurement, and Control*, Series G, Vol. 94, Dec. 1972, pp. 323–329.

[29]Isidori, A., *Nonlinear Control Systems*, Springer–Verlag, Berlin, 1989.

[30]Stengel, R. F., "Toward Intelligent Flight Control," *IEEE Transactions on Systems, Man, and Cybernetics*, Vol. 23, No. 6, 1993, pp. 1699–1717.

[31]Chow, J., and Kokotovic, P., "Two-Time-Scale Feedback Design of a Class of Nonlinear Systems," *IEEE Transactions on Automatic Control*, Vol. AC-23, No. 3, 1978.

[32]Etkin, B., *Dynamics of Atmospheric Flight*, Wiley, New York, 1972.

[33]Lane, S., "Theory and Development of Adaptive Flight Control Systems Using Nonlinear Inverse Dynamics," Ph.D. Dissertation, Princeton Univ., Princeton, NJ, 1988 (Rept. No. 1806-T).

[34]Van Buren, M. A., and Mease, K. D., "Aerospace Plane Guidance Using Time-Scale Decomposition: A Geometric Approach," *Proceedings of the 1991 AIAA Guidance, Navigation, and Control Conference*, AIAA, Washington, DC, Vol. 1, pp. 370–379.

[35]Mulgund, S. S., and Stengel, R. F., "Optimal Nonlinear Estimation for Aircraft Flight Control in Wind Shear," *Proceedings of the 1994 Congress of the International Council of Astronautical Sciences*, Anaheim, CA, 1994, pp. 1747–1755.

[36]Zhao, Y., and Bryson, A. E., "Approach Guidance in a Downburst," *Journal of Guidance, Control, and Dynamics*, Vol. 15, No. 4, 1992, pp. 893–900.

[37]Jacobson, D. H., and Lele, M. M., "A Transformation Technique for Optimal Control Problems with a State Variable Inequality Constraint," *IEEE Transactions on Automatic Control*, Vol. AC-14, No. 5, 1969.

[38]Ostroff, A. J., et al., "Evaluation of a Total Energy-Rate Sensor on a Transport Airplane," NASA TP-2212, 1983.

[39]Gelb, A. (ed.), *Applied Optimal Estimation*, MIT Press, Cambridge, MA, 1974.